https://ntrs.nasa.gov/search.jsp?R=20190026529 2020-03-11T00:48:27+00:00Z

Proceedings of ASME Turbo Expo 2019: Turbomachinery Technical Conference and Exposition
GT2019
June 17 - 21, 2019, Phoenix, Arizona, USA

GT2019-90002

ANALYSIS OF THE HONEYWELL UNCERTIFIED RESEARCH ENGINE (HURE) WITH ICE CRYSTAL CLOUD INGESTION AT SIMULATED ALTITUDES

Joseph P. Veres, Philip C.E. Jorgenson, Samaun Nili, Shashwath R. Bommireddy, Kenneth L. Suder
National Aeronautics and Space Administration, Glenn Research Center
Cleveland, Ohio, USA

ABSTRACT

The Honeywell Uncertified Research Engine (HURE), a research version of a turbofan engine that never entered production, was tested in the NASA Propulsion System Laboratory (PSL), an altitude test facility at the NASA Glenn Research Center. The PSL is a facility that is equipped with water spray bars capable of producing an ice cloud consisting of ice particles, having a controlled particle diameter and concentration in the air flow. To develop the test matrix of the HURE, numerical analysis of flow and ice particle thermodynamics was performed on the compression system of the turbofan engine to predict operating conditions that could potentially result in a risk of ice accretion due to ice crystal ingestion. The goal of the test matrix was to have ice accrete in two regions of the compression system: region one, which consists of the fan-stator through the inlet guide vane (IGV), and region two which is the first stator within the high pressure compressor. The predictive analyses were performed with the mean line compressor flow modeling code (COMDES-MELT) which includes an ice particle model.

The HURE engine was tested in PSL with the ice cloud over the range of operating conditions of altitude, ambient temperature, simulated flight Mach number, and fan speed with guidance from the analytical predictions. The engine was fitted with video cameras at strategic locations within the engine compression system flow path where ice was predicted to accrete, in order to visually confirm ice accretion when it occurred. In addition, traditional compressor instrumentation such as total pressure and temperature probes, static pressure taps, and metal temperature thermocouples were installed in targeted areas where the risk of ice accretion was expected.

The current research focuses on the analysis of the data that was obtained after testing the HURE engine in PSL with ice crystal ingestion. The computational method (COMDES-MELT) was enhanced by computing key parameters through the fan-stator at multiple span wise locations, in order to increase the fidelity with the current mean-line method. The Icing Wedge static wet bulb temperature thresholds were applicable for determining the risk of ice accretion in the fan-stator, which is thought to be an adiabatic region. At some operating conditions near the splitter-lip region, other sources of heat (non-adiabatic walls) were suspected to be the cause of accretion, and the Icing Wedge was not applicable to predict accretion at that location. A simple order-of-magnitude heat transfer model was implemented into the COMDES-MELT code to estimate the wall temperature minimum and maximum thresholds that support ice accretion, as observed by video confirmation. The results from this model spanned the range of wall temperatures measured on a previous engine that experienced ice accretion at certain operating conditions.

INTRODUCTION

Ice crystals ingested into turbofan engines during the operation of commercial aircraft at high altitudes can result in ice accretion in the compression system (Refs. 1, 2). As ice crystals are ingested into the fan, a portion of the ice crystals melt due to the rising static temperature of the air. It is hypothesized that the ice-water mixture then impacts and cools the surfaces through evaporation and ultimately ice accretes on the compressor components. The accreted ice can cause one or more of the following modes of failure: uncommanded loss of thrust control, compressor surge or stall, ice shedding which can result in structural damage to the compressor blades, and possible combustor flameout. To improve understanding of the causes of ice accretion within an engine, full engine testing with ice crystal ingestion has been performed in the NASA Propulsion Systems Laboratory (PSL) (Refs. 3, 4, 5), as well as fundamental ice crystal testing (Refs. 6, 7).

This study focuses on the analysis of the test data obtained from the Honeywell Uncertified Research Engine (HURE). The engine was tested in the PSL with ice crystal cloud ingestion over a range of simulated altitudes and operating conditions. The test took place in January 2018, as part of the engine icing research supported by the NASA Advanced Aircraft Icing Subproject, under the NASA Advanced Air Transport Technology Project.

Since the HURE was never in production, it has not experienced in-flight events that have been attributed to ice crystal ingestion. The engine was installed into the PSL altitude facility with a direct connect duct that mates to the engine flange, such that it utilizes the full flow capacity of the PSL altitude wind tunnel as illustrated in the right photo of Figure 1. There was no flight nacelle installed in this test configuration. The PSL is an altitude engine testing facility located at NASA Glenn Research Center. The PSL features the Escort data acquisition system. Each engine data point is stored in the system and is referred to as an Escort data point number. The Escort system records the data at a frequency of approximately one scan per second. This test facility features water spray bars that can produce a fully glaciated ice crystal cloud with controllable ice particle size and concentration per unit volume of air. The spray bars (left photo) and the direct-connect inlet duct piping are shown below in Figure 1 with the engine and test stand (right photo).

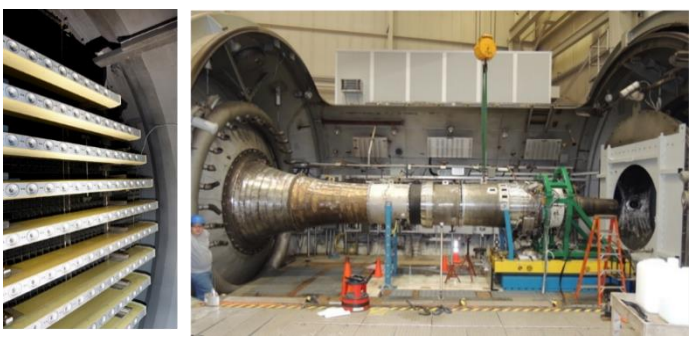

Figure 1. Engine Testing in PSL at Simulated Altitude and ice crystals. Direct connect duct (right), spray bars (left).

The purpose of the test was to determine if ice would accrete within the compressor components at the predicted operating conditions outlined in Reference 8. The HURE engine (cross-section illustrated in Figure 2) was heavily instrumented with traditional pressure and temperature gauges, as well as video cameras aft of the fan and near the splitter-lip, as well as inlet guide vane (IGV) regions.

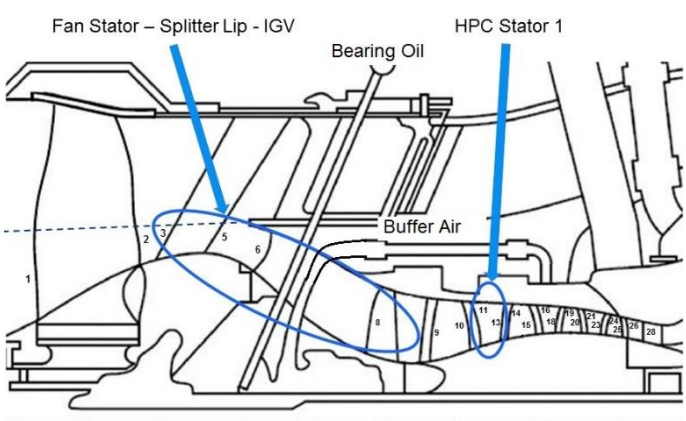

Figure 2. Honeywell Uncertified Research Engine (Courtesy Honeywell Engines).

Prior to the test, an extensive study utilizing a mean-line compressor flow analysis code was performed to determine the operating conditions where a risk of ice accretion would be expected (Ref. 8). The study resulted in numerous operating conditions and altitudes where the ice would be expected to form, at several locations within the compression system. The computational tool that was utilized consisted of an enhanced version of the COMDES compressor flow code (Ref. 9). This tool was previously applied to analyze icing data from other engines tested in PSL with ice crystal ingestion (Refs. 10-16). That research resulted in determining values for key parameters that can indicate whether there is a risk of ice accretion. These key parameters form the basis of the Icing Wedge. The Icing Wedge is defined by thresholds of static wet bulb temperature, ice-water flow rate to air flow rate, and a non-zero particle melt ratio. Leveraging from the previous analytical studies, it was hypothesized in Reference 8 that the Icing Wedge is universally applicable to other turbofan engines. The primary focus of the study in Reference 8 was to determine the engine operating conditions and ambient temperatures at various altitudes, that would result in ice accretion between the fan-stator, splitter-lip, and the inlet guide vane (IGV) of the high-pressure compressor (HPC). The secondary focus of that study was to enable accretion to occur in the variable stator of the HPC first stage (stator 1), however this analysis is not included in this paper, but is included in References 17 and 18. These targeted areas where the ice was expected to occur and the associated station numbers from the compressor flow simulation are illustrated in Figure 2.

The current study is focused on the analysis of 57 Escort test points that were taken at distinct operating conditions in PSL at altitudes between 5K and 45K feet. The computer analyses results for these data points with the Customer Deck as well as with the COMDES-MELT codes are listed in the Appendices A, B, and C in Reference 17. The results of the HURE testing confirmed by the video that ice accreted and, or collected at all altitudes in the general targeted regions of the fan-stator, splitter-lip, and the IGV, confirming most of the predictions made in Reference 8. During testing, it was observed that ice accreted at the fan-stator in accordance with the icing parameter thresholds governed by the Icing Wedge. Note that this fan-rotor is highly loaded, causing a significant rise in total temperature, which is adequate to partially melt the incoming ice particles.

Ice accretion was observed on the front frame components near the splitter-lip at lower static wet bulb temperatures than was expected, based on the Icing Wedge minimum threshold of 492R. In addition, the accretion occurred at static air temperatures well below freezing, thus no particle melting could have occurred due to heating from the air alone. The aluminum front frame may have received heat from additional sources besides the air, but this process is not well understood for this engine. It is possible that the ice accretion in that region was not an adiabatic process. During testing, in order to compensate for the lack of a heat transfer model in the COMDES-MELT code, the target static wet bulb temperature (Twbs) for ice to accrete in the front frame region was reduced to 468R. This was 24R below the Icing Wedge minimum threshold of 492R. The new target

Twbs was determined by the analysis of one of the operating points where ice accreted at the splitter-lip and shroud region. Using COMDES-MELT, new testing conditions were rapidly derived prior to further testing, and the test matrix was modified. This was successful in enabling ice to accrete in the front frame components (splitter-lip and shroud region). For post-test data analysis, a simple bulk heat transfer model was developed to estimate the wall metal surface temperature. This was done in order to compare it to previous engine tests which had measured wall temperatures between 492R to 501R during ice accretion.

Video observation indicated that ice collected on the variable inlet guide vane (IGV) of the high-pressure compressor. This may have been due to partially melted particles flowing along the shroud wall from upstream, that collected on the IGV surface. This appeared to be different from the ice accretion observed at the upstream regions. Due to the possible non-adiabatic process upstream of the IGV, the Icing Wedge thresholds, as an indicator of accretion risk, are not applicable in this region.

The testing of the HURE indicated that ice accreted or collected at all altitudes tested and was confirmed by video cameras at the three targeted locations of fan-stator, splitter-lip-strut, and IGV. Note that the accretion in those locations occurred at different operating conditions. Those test points are superimposed onto the historical engine icing events reported in References 1 and 2, as illustrated in Figure 3. The historical icing events occurred on commercial airlines (Figure 3) during flight through clouds with high ice-water content. Those events have been attributed to ice crystal ingestion and subsequent ice buildup in the engine, but the exact location within the compression system is unknown. The plot in Figure 3 includes reference lines indicating the International Standard Atmosphere (ISA) temperature, with +18F and +36F above ISA, versus altitude. Ice accretion within the HURE engine spanned the entire range of the reported historical icing events for commercial engines. The PSL test conditions at 5K feet altitude were set to inlet temperatures on the order of -25F, which are offset by -45F from the ISA temperature, in order to induce ice accretion in the targeted location of the compression system. Note that this condition does not occur in nature, but was artificially set in PSL for icing research and code modeling development.

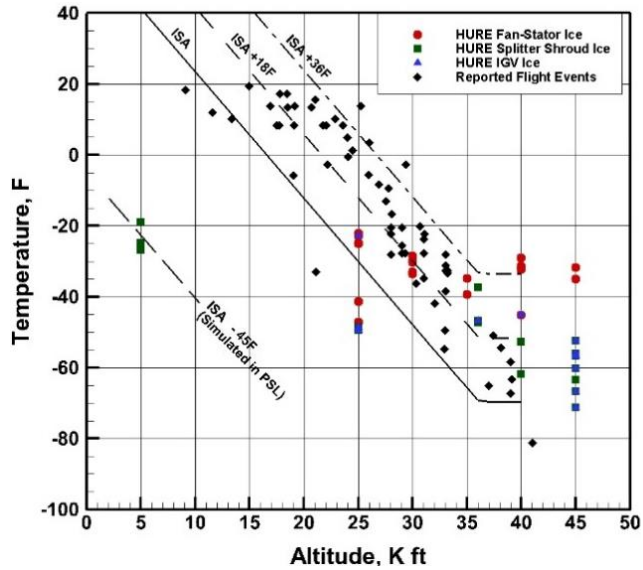

Figure 3. The confirmed operating points with ice accretion or collection in the HURE engine during PSL testing, superimposed onto the reported commercial engine icing events (Ref. 1).

Post-test analysis showed differences between the engine thermodynamic system model and the measured engine performance data. These comparisons between the system model and the tested engine performance were based on data prior to ice-cloud ingestion. These variances that were on the order of 6% may be partially responsible for uncertainties in the post-test analyses with the COMDES-MELT code, which depends on the engine system model as well as the measured test data for boundary conditions.

NOMENCLATURE

CD	customer deck
Delta ISA	offset temperature from ISA
ISA	International Standard Atmosphere
IWAR	ice-water flow rate to air flow rate ratio
IWC	ice water content (glaciated crystals), g/m3
m	mass flow rate of air, lbm/s
PT1	engine inlet total pressure
Tamb	ambient temperature, static
TT1	engine inlet total temperature
Twbs	static wet bulb temperature
u	micron

COMPRESSOR CODE CALIBRATION

Prior to testing in PSL, the COMDES code was compared to the design point performance results from a customer deck, as well as more detailed results from a two-dimensional streamline-curvature analysis code for the fan and the four axial compressor stages of the HPC. These two results were provided by Honeywell for the purpose of calibrating the COMDES code at the design point. These are listed in Appendix A of Reference 17, and include the summary of the HURE fan and HPC geometry,

as well as the streamline-curvature analysis results, and the COMDES flow code results at each blade edge.

After testing the HURE engine, in order to further verify the accuracy of the COMDES compressor code in being able to model the flow through the full fan and fan-core region, six test data points without ice cloud ingestion were analyzed with the COMDES code (Appendix B of Ref. 17). The purpose was to confirm that the compressor aerodynamic performance predicted by the flow model matched the measured aerodynamic performance test data of the compressor within the engine. In addition to calibrating the rotor and stator losses within the flow model, the effects of the aerodynamic instrumentation installed in the compression system could also potentially influence the measured performance. The effect of the instrumentation was not significant, since the measured and the fan and compressor aero performance (total temperature and pressure, and static pressure) modeled with the CD and COMDES were all in good general agreement (see Figures 42-47 in Appendix B of Ref. 17). Therefore there was no compressor code calibration required to accurately model the fan, flow splitter, and IGV regions. During testing even in an ice cloud environment, it was observed that the total pressure and the wall static pressure measurements in the fan-stator and core strut regions remained unaffected by the particles. However, the cascading aerodynamic effects of even small differences in the fan performance can propagate through the HPC and affect the compressor exit conditions (Pt and Tt) through the stage matching. This effect may be responsible for the observed differences in engine performance parameters of up to 6% between the CD engine system model and measured Escort test data. Even though the compressor exit plane is well downstream of any ice accretion sites, the differences in conditions there may influence the calculation of core mass flow in the CD system model.

FAN-STATOR ANALYSIS; RISK OF ACCRETION GOVERNED BY THE ICING WEDGE THRESHOLDS

The analysis of the HURE test data was performed with the similar computational process shown in Figure 4 that was utilized in the predictions of icing risk of Reference 8. The computational process is further detailed in Appendix C of Reference 17, with the description of the input parameters for the engine thermodynamic cycle code (CD) as well as for the COMDES-MELT code. Initially the CD is executed at the tested altitude, ambient temperature, flight Mach number, and fan speed. The results from the engine CD model are utilized as boundary conditions to the subsequent execution of the compressor flow analysis code (COMDES-MELT). The compressor flow analysis is performed to determine the aerodynamic flow field as well as the thermodynamic state of the ice particle, in addition to computing the key icing parameters of wet bulb temperature and IWAR. These analyses assumed that the ice particles were distributed uniformly through the bypass as well as the engine core, even though this engine has a "hidden core." As part of the ice particle thermodynamic state, the melt ratio is calculated to determine the existence of liquid water content, which is a requirement for there to be ice accretion. Since there is no particle break up model in the code, the analyses was performed over a range of possible particle sizes from 3 – 10 microns.

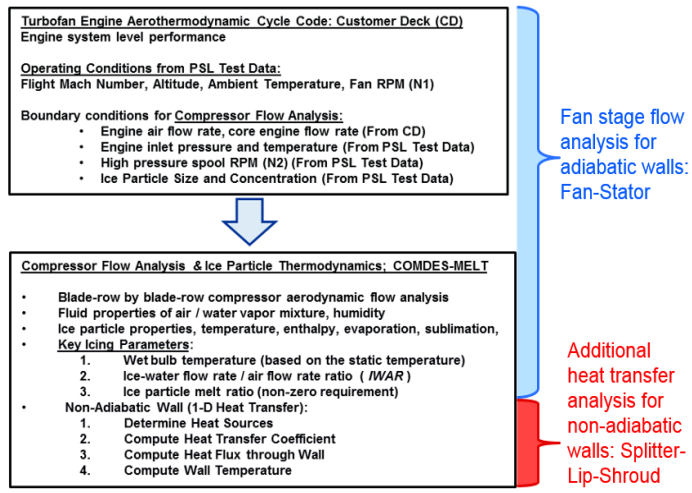

Figure 4. Computational process for the test data analysis for the fan stage of the HURE turbofan engine

The calculated icing parameters are then compared to the minimum and maximum threshold limits of the Icing Wedge shown in Figure 5 and the video images of the compressor components are evaluated to determine if ice accreted on the component. Note that the 3-dimensional Icing Wedge shown in Figure 5 was derived from a previous turbofan engine test, where the blockage growth rate due to ice accretion was iteratively determined to match the measured wall static pressure and the total pressure ratio. This study only utilizes the minimum and maximum threshold values of the static wet bulb temperature (Twbs) of the Icing Wedge that indicate the risk of accretion on the fan-stator. Estimates of blockage growth rate due to accretion and boundary layer growth are not part of this current study.

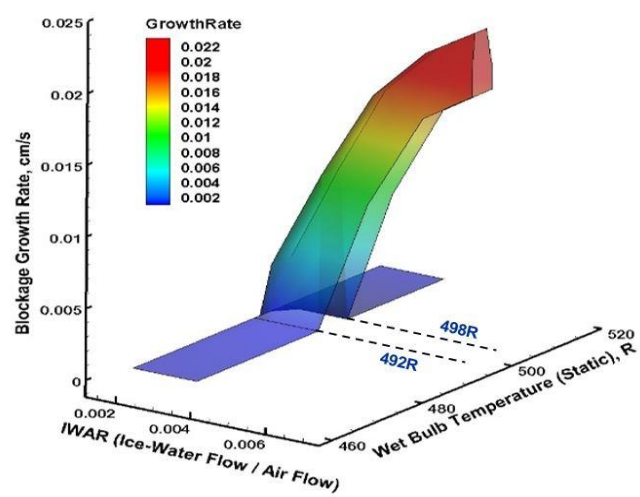

Figure 5. The Icing Wedge defined by the thresholds of Twbs between 492R – 498R for a risk of accretion (Reference 16).

The values of the static wet bulb temperature (Twbs) in the fan-stator are utilized as a verification of accuracy for predicting the risk of ice accretion. If the value of Twbs falls between the Icing Wedge thresholds, then there is a risk of ice accretion. The static wet bulb temperature is calculated from the local values of static air temperature and the relative humidity.

The location of ice accretion on the fan-stator was observed in the video to be at discrete radial locations at each operating condition (Escort test point), but for some test points the accretion appeared to be at a higher span than the notional streamline of the fan-core. It became apparent that a full fan flow analysis was also required to determine the Twbs at the higher RMS radius of the full fan.

For this reason two models were created of the fan-stator. The first model was of the full fan-rotor and fan-stator. This analysis resulted in computing the aerodynamic parameters at the root-mean-square (RMS) radius of the full fan stage, as illustrated in Figure 6. The computed parameters included: relative and absolute velocities, static and total pressures and temperatures, absolute and relative flow angles, including the static wet bulb temperature and the particle melt ratio at the leading and trailing edges. The second model was of the fan-core region through the splitter-lip, and the variable IGV. In this analysis, a notional stream line was assumed that divided the flow between the bypass and the core, as illustrated in Figure 6. The notional streamline was used as the fan-core flow path outer wall. Likewise that analysis resulted in modeling all the aerodynamic parameters, including the static wet bulb temperature (Twbs) and the particle melt ratio at the RMS radius of the fan-core stage, through the IGV.

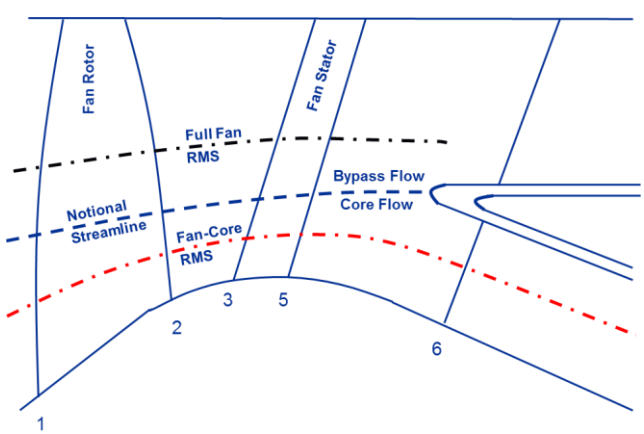

Figure 6. Two flow models of the fan stage: (a) Full fan; (b) Fan-core, with its outer flow path wall indicated by the notional streamline. The numbers 1 – 6 refer to the meridional stations.

The computed Twbs and IWAR of the Escort test points analyzed in the fan stator region are illustrated in Figure 7. The symbols connected by dotted lines represent the values of Twbs at the full fan and at the fan-core RMS radii. The span wise work distribution in the fan rotor resulted in a gradient of static temperature, resulting in a large variation of Twbs. The minimum and maximum Twbs thresholds (492R – 498R) of the Icing Wedge from Reference 16 are represented by two horizontal lines. These are superimposed onto the calculated values of Twbs obtained from the HURE test data analyses. Figure 7 represents the static wet bulb temperature at station 5 shown in Figure 6.

The black symbols in Figure 7 indicate the Escort test points where ice accretion on the fan stator was confirmed by video observation. For most of the test points that experienced accretion, the range of Twbs spanned the minimum and maximum thresholds of the Icing Wedge. The combined analysis of the fan-core and full fan results had a 94% success rate of spanning the Icing Wedge for all data points analyzed which had ice accretion in the fan-stator.

The test data points where ice accretion was not observed by video in the fan-stator, were outside the Icing Wedge thresholds, as indicated by the red symbols in Figure 7. The analysis results had a 100% success rate of being outside the Icing Wedge for all data points analyzed which had no ice accretion in the fan-stator.

In summary, there was good agreement between the Twbs thresholds of the Icing Wedge and the analysis of the HURE test results. However, it was necessary to have both the full fan and the fan-core models to determine the range of Twbs along the full span of the fan-stator.

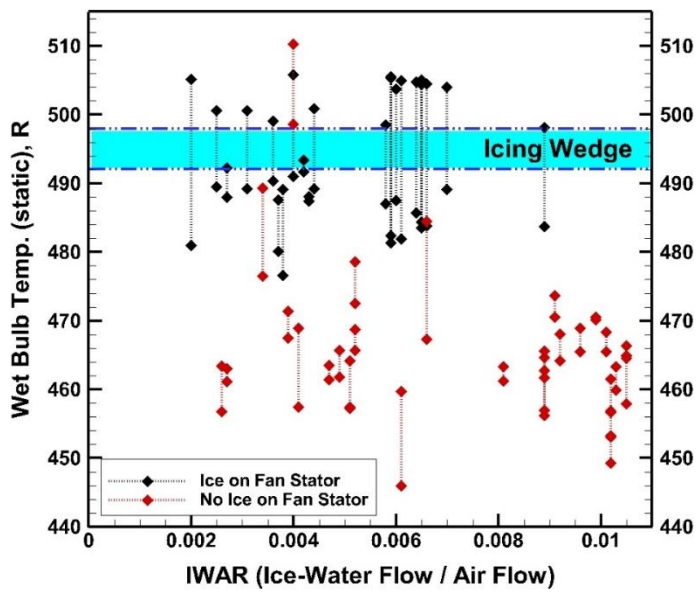

Figure 7. Range of static wet bulb temperature at the fan-core stator and full fan-stator root-mean-square radii, relative to the Icing Wedge thresholds.

The static wet bulb temperature is based on accurate calculations of the local static air temperature as well as the local relative humidity within the flow field of the fan as well as the four axial stages in the core. A sample data point is shown in Figure 8, where the inlet relative humidity is 100%, illustrates the rapid drop in relative humidity. The specific humidity increases due to the sublimation, melting, and evaporation of the ice particles. The accretion at station 5 (fan-stator trailing edge) occurs at approximately 10% relative humidity as shown in Figure 8.

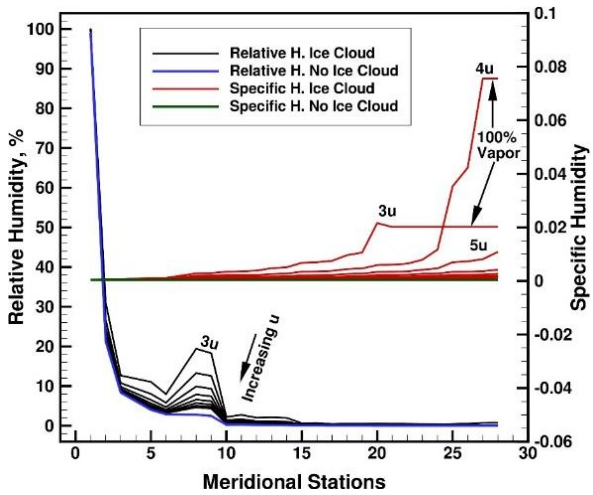

Figure 8. Distribution of relative and specific humidity.

The operating conditions for two sample Escort data points are listed in Table 1. Escort data point 121 is the case with ice accretion in the fan-stator, while Escort data point 287 had no ice accretion. The computer analyses results for all the data points analyzed with the Customer Deck as well as with the COMDES-MELT codes are included in Appendix C of Reference 17 and listed by Escort data point number. These include all data points with and without ice accretion in the fan-stator.

Table 1: Fan-Stator: Ice Accretion (121); No Ice Accretion (287)

Escort Data Point	Altitude, K ft	Flight Mach Number	Ambient Temp, R	Tt PSL Station 1 Ice Cloud On, R	Pt PSL Station 1, psia	Ice Water Content (IWC)	IWAR	Twbs Fan Core & Full Fan-Stator, Station 5, 5 microns	Melt Ratio, Station 5, 5 micron
121	45	0.81	427	484	3.28	1.48	0.0058	487- 498	0.0 - 0.16
287	36	0.61	412	443	4.22	2.48	0.0066	467- 484	0.0 - 0.0

The above Tables 1 show the static wet bulb temperature and the corresponding particle melt ratio for a 5 micron particle at the trailing edge of the fan-stator.

Figure 9 shows the view of the fan-stator from the video camera mounted on the engine shroud facing radially inward towards the hub. The image shows a typical case (Escort 121) where the ice accretion was observed on the fan-stator through the video cameras.

Figure 9. Video camera view of the fan-stator showing that ice accretion occurred there during Escort data 121.

Figure 10 illustrates the static wet bulb temperature distribution for Escort data point 121 through the full fan (represented by blue lines), and the fan-core and the four stage axial compressor (represented by black lines), as well as the particle melt ratio, over a range of particle size from 3-10 microns.

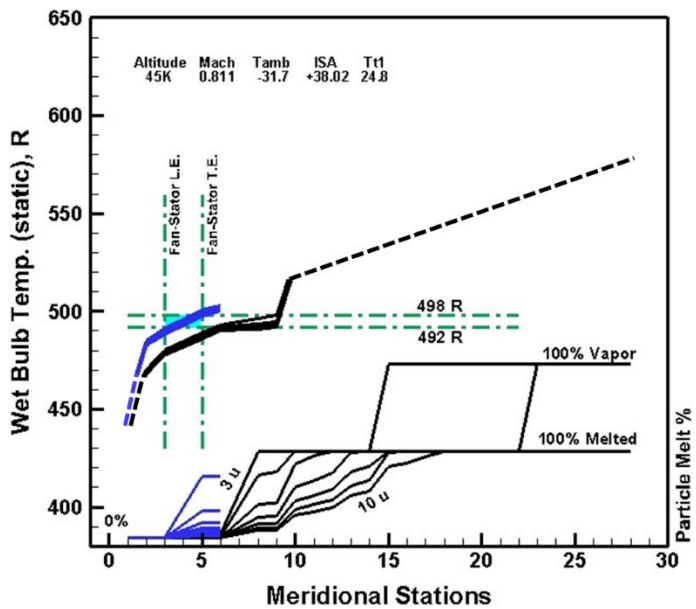

Figure 10. Ice accretion occurred in the fan-stator during Escort 121. The static wet bulb temperature was within the Icing Wedge.

The range of particle sizes analyzed with COMDES-MELT in Figure 10 were between 3 and 10 microns for all the stations in the flow path. The full fan model had 5 meridional stations, while the fan-core model is comprised of 28 meridional stations, as shown in Figure 2, since the four axial stages of the high pressure compressor were also included as part of the flow analysis. The calculated Twbs downstream of the HPC rotor 1

(meridional station 9) was significantly higher than the maximum threshold of the Icing Wedge. Therefore there was no risk of accretion in the downstream stages, although there were no video cameras in those stages for visual confirmation. For the Escort data points where ice accretion occurred on the fan-stator, there was no accretion observed concurrently on the splitter-lip, shroud, strut, IGV regions. Likewise, when ice accretion was observed in the splitter-lip, shroud, strut, IGV regions, there was no accretion observed concurrently on the fan-stator.

SPLITTER – LIP - STRUT – GOOSENECK REGION; NON-ADIABATIC WALL

PSL Test, and Real-Time Predictions of Ice Accretion Operating Points:

Early in the HURE testing, it was observed that at several of the tested operating points, ice accretion in the front frame region (splitter, shroud, gooseneck and support strut) did not occur as expected even though the static wet bulb temperatures (Twbs) were within the thresholds of the Icing Wedge. Although there were no metal thermocouples to measure the wall temperature near the aluminum splitter-shroud region, it is assumed that the metal temperatures were above freezing, since liquid water streaks were observed in the videos on the shroud. The target static wet bulb temperature was reduced by 24R from the Icing Wedge minimum threshold value of 492R in order to accrete ice in the region of the front frame. The value of 468R was determined through flow modeling in near real-time analysis of several test data points that experienced ice accretion at the splitter-shroud region. Flow analysis of those data points indicated that the calculated static air temperature was well below freezing at this location. Thus no melting could have possibly occurred solely due to the heat of compression caused by the fan. In addition, the calculated temperature of the ice particles was also well below freezing, based on the flow analysis.

New testing operating conditions over a wide range of simulated altitudes were rapidly determined utilizing the lower Twbs threshold in the splitter-shroud region prior to further testing, and the test plan was modified accordingly. With these updated conditions ice began to accrete within seconds after the ice cloud was initiated. It was assumed that the splitter-shroud region wall temperatures at this condition were near freezing, since the measured metal temperatures on the IGV were at freezing. This technique was successful in inducing ice to accrete in the splitter-shroud region, for most subsequent tested operating points. Note that when ice accretion was observed in the splitter-lip-strut, shroud region there was no accretion observed on the fan-stator at the same operating points.

The aluminum front frame may have received heat from additional sources besides the air, in order to partially melt the particles, which then subsequently accreted near the splitter-lip-shroud. A physics-based explanation was sought for this phenomenon. It is possible that the ice accretion in this region is due to a non-adiabatic wall. Although the source of additional heat flux is not completely understood, a simple order-of-magnitude heat flux model was implemented in COMDES-MELT to estimate the wall temperature in this region.

Order-of-Magnitude Estimate of Wall Temperature:

In order to reconcile the additional enthalpy from the non-adiabatic flow path wall, an order-of-magnitude method was implemented that assumes a continuous supply of heat which is transferred directly to the ice particle by conduction. The heat transfer model was calibrated empirically based on the HURE test results. Since there were no thermocouples in the splitter-shroud region of the front frame where ice accreted, it was necessary to utilize measured IGV metal temperature test data to develop the heat transfer model for the front frame. The purpose of the heat transfer model was to calculate the wall temperature in the splitter-shroud region. Several data points were observed to have glassy ice accretion at the splitter-lip and shroud of the gooseneck with no shedding (hard ice). At these operating points it was observed that the measured metal temperatures at the IGV were near 492R. It was therefore assumed that the metal temperature at the splitter-lip and shroud were likewise near 492R at these operating conditions. Table 2 below lists four test data points at various altitudes that were used to confirm that when hard ice was observed to accrete on the splitter-lip and (or) the shroud, the IGV had a measured metal temperature near 492R. This was also observed in the previous engine test (Ref. 15, shown in Figure 11). The total air temperature at the splitter-shroud region was approximately the same in the CD and COMDES models, and confirmed by the measured Escort data. The calculated static air temperature in the splitter-shroud region as modeled by COMDES was consistently below freezing. Yet it was observed that ice accreted in the splitter-strut-shroud region.

Table 2 Calibration of the Heat Transfer Model in COMDES-MELT

Test Data Point, Escort	Altitude, K ft	Splitter-Shroud Ttotal Air, CD, Escort & COMDES, R	Splitter-Shroud Tstatic Air COMDES, R	Tigv Metal Pre Ice Cloud, R	Tigv Metal Post Ice Cloud; After 60 sec, R
156	45	509.4	486.3	511.2	492.3
283	36	499.9	481.9	501. 1	491.0
279	25	496.1	478.1	494.2	491.9
242	5	492.8	476.9	492.0	491.9

A simple heat transfer model was created, where the initial unknown was the bulk heat transfer coefficient at the splitter-shroud flow path wall, $h_{wall\ plenum}$. To estimate $h_{wall\ plenum}$, two of the test data points were selected (156 and 283) which had visual confirmation of glassy, hard ice accretion which did not shed, on the splitter-lip and shroud. Although the exact source of heat (enthalpy) to the walls was not known, in this study it is assumed that the heated air from a downstream stage was the source. In order to have this additional enthalpy vary with engine operating conditions, for modeling purposes it was assumed that the source was the HPC stage 2 exit (COMDES-MELT; *Tt2*).

In the analysis that follows, the temperature of the plenum, $T_{wall\ plenum}$, was assumed to be the same as *Tt2*. At the selected data points (156 and 283), the heat flux, *Q*, was calculated assuming that the splitter and shroud wall temperatures, $T_{wall\ core}$, were at 492R with the following equation (1), where the *m* is the mass flow rate of the ice particles going through the engine core.

$$Q = SHC * m * (T_{particle} - T_{wall\ core}) \quad (1)$$

The mass flow of ice particles through the engine core is assumed to be proportional to the air flow rate, since the compressor code lacked a model to track the particle distribution within the flow path in three-dimensional space. The *SHC* is the specific heat capacity of the ice particles. The ice particle temperature was obtained from an initial solution of the COMDES-MELT code. Knowing the heat flux, *Q*, the temperature on the plenum side of the shroud wall, $T_{wall\ plenum}$, was computed with equation (2) .

$$T_{wall\ plenum} = Q * \frac{Thickness}{(A * k)} + T_{wall\ core} \quad (2)$$

The *A* in the above equation is the surface area of the splitter-shroud region through the entire goose neck, while *k* is the coefficient of conduction for aluminum, and thickness is the average wall thickness of the aluminum shroud casing. The bulk heat transfer coefficient, $h_{wall\ plenum}$ was determined for this engine based on the assumption of wall temperature of 492R with equation (3).

$$h_{wall\ plenum} = \frac{Q}{A * (T_{wall\ plenum} - T_{air\ plenum})} \quad (3)$$

For the flow analysis of all other data points, the bulk heat transfer coefficient was assumed to remain at the value which was calculated from the data points 156 and 283 of Table 2. The above three equations were incorporated into COMDES-MELT and are solved for the three unknown parameters (*Q*, $T_{wall\ plenum}$, $T_{wall\ core}$) for all subsequent data points analyzed in this study. COMDES-MELT was executed iteratively to first, determine $T_{wall\ plenum}$ (*Tt2*) and particle temperature at the splitter – shroud region, and finally executed to calculate the splitter – shroud wall temperature ($T_{wall\ core}$). However, in the current study the enthalpy extracted from the heated wall was not transferred back to the ice particle to determine its thermodynamic state once it made contact with the heated splitter-shroud wall. The computational process summarizing the steps above is outlined in Figure 4 and in Appendix C of Reference 17.

The computed value of $T_{wall\ core}$ was then compared to previous engine test data (Honeywell ALF502R-5, serial number LF11) with measured wall metal temperatures at the location where there was significant ice accretion (Ref. 15) and are illustrated in Figure 11. Note that additional analysis of the engine data in Reference 15 was performed as part of this study, and is illustrated in Figure 11. Ice accretion occurred on the LF11 compressor shroud wall at measured metal temperatures on the shroud wall between 493R and 501R.

The range of calculated metal wall temperatures ($T_{wall\ core}$) at the splitter-shroud region using this heat transfer model where ice accretion was confirmed by video, were between 475R to 519R, and span the range of wall temperatures measured in the LF11 engine during accretion. The calculated HURE wall temperatures (solid blue circles) were superimposed onto the measured wall temperatures (black diamonds) of the LF11 engine that supported ice accretion. The calculated wall temperature increases with reduced IWAR, and is in agreement with the trend observed in the previous engine test. The solid green circles were ice accretion data points from HURE at the 5K altitude.

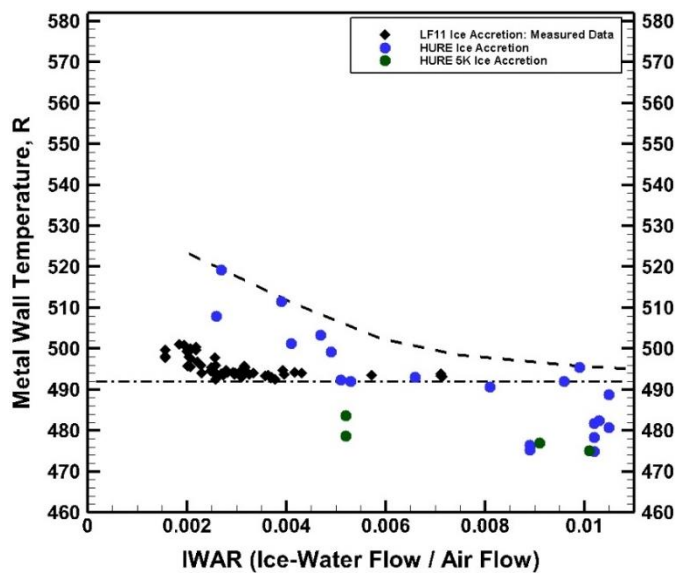

Figure 11. Calculated wall temperature versus IWAR of the HURE splitter-shroud region for data points with ice accretion at high altitudes and at 5K ft, compared to the measured wall temperature of the LF11 engine (Ref. 15).

Escort data point 153 and 156 are examples of the two distinct types of ice accretion in the splitter-shroud region in which ice accreted with horns on the splitter-lip (Escort 153, Figure 12), and without ice horns on the splitter but ice on the shroud (Escort 156, Figure 13). The ice accreted at discrete circumferential locations. For Escort data point 156, the compressor flow model was executed to determine the static wet bulb temperature distribution through the full fan, the fan-core and the four stage axial compressor, as well as the particle melt ratio over a range of particle size for 3 – 10 microns, and is illustrated in Figure 14. The flow model indicated that the splitter-lip-shroud surface wet bulb temperature was 24R below the Icing Wedge minimum threshold of 492R. The flow model for Escort data point 153 (ice horns on the splitter-lip) indicated that surface wet bulb temperature at that location was 19R below the Icing Wedge minimum threshold.

Figure 12. Escort 153. Ice accretion with ice horns on the splitter-lip at discrete circumferential locations.

Figure 13. For Escort 156, there was ice accretion on the shroud, without horns on the splitter-lip.

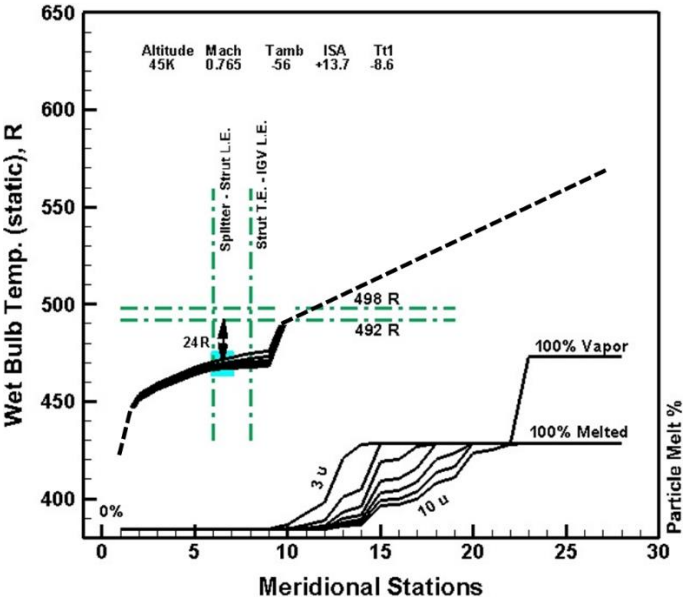

Figure 14. Ice accretion occurred at Escort 156. The static wet bulb temperature is 24R below the Icing Wedge minimum threshold of 492R.

Table 3 Splitter-Lip-Shroud: Sample Ice Accretion Points

Escort Data Point	Altitude, K ft	Flight Mach	Ambient Temp., R	Tt PSL Station 1 Ice Cloud ON, R	Pt PSL Station1, psia	Ice Water Content (IWC)	IWAR	Twbs Splitter, Shroud, Fan Core (6), 5 microns	T wall Core after 60s (6) 2.1, R
153	45	0.81	399.4	452.2	3.28	2.89	0.0099	473.1	495.5
156	45	0.77	403.6	451.0	3.13	2.73	0.0096	467.9	492.0

A third type of icing on the splitter-lip occurred, which was a rapid collection and shedding at frequencies of multiple times per second. The ice appeared as small white "mounds" which were quite different from the glassy hard ice noted in Figures 12 and 13. These mounds also appeared at circumferentially discrete locations on the splitter-lip. The calculated metal temperatures for these data points were in the range from 505.4R to 563.9R, which is significantly higher than the glassy hard ice accretion cases.

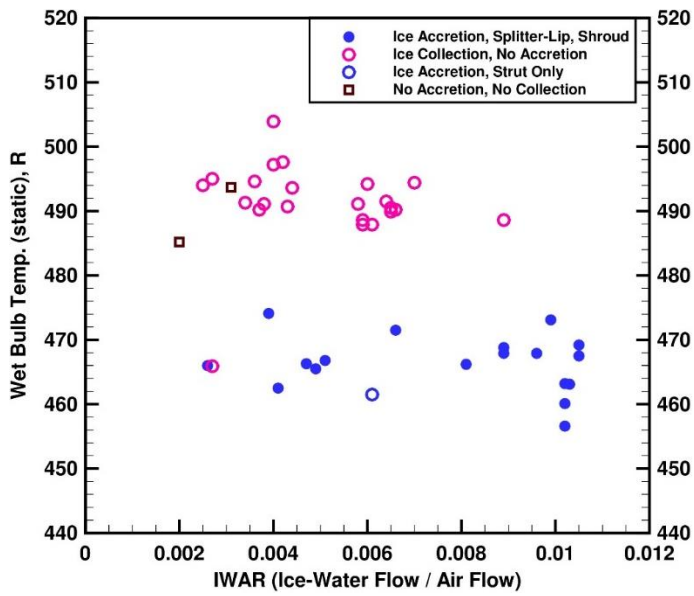

Figure 15. The static wet bulb temperature versus IWAR in the splitter-shroud region, for the cases with hard ice accretion and those with only collection and rapid shedding.

The range of Twbs for the cases with collection (pink open symbols in Figure 15), but no accretion was from 487.9R to 503.9R. This spans the Icing Wedge thresholds, however the Icing Wedge thresholds do not apply here due to the additional heat flux from the walls to the ice particles.

Figure 16 illustrates the strong effect of the local air static temperature on the ice accretion potential in the splitter-shroud region. The higher air temperatures (pink open symbols) result in the collection of ice on the splitter-lip, with rapid shedding a

rate of several times per second, to several seconds per shed, with no accretion of hard glassy ice. The closed black symbols are hard glassy ice accretion on the splitter lip, at calculated wall temperatures between 475R – 519R. To accurately model this heat flux from the wall to the ice particle, as well as other potential heat sources, a high fidelity multi-disciplinary model of the entire front frame would be required that includes fluid dynamic analysis as well as conjugate heat transfer.

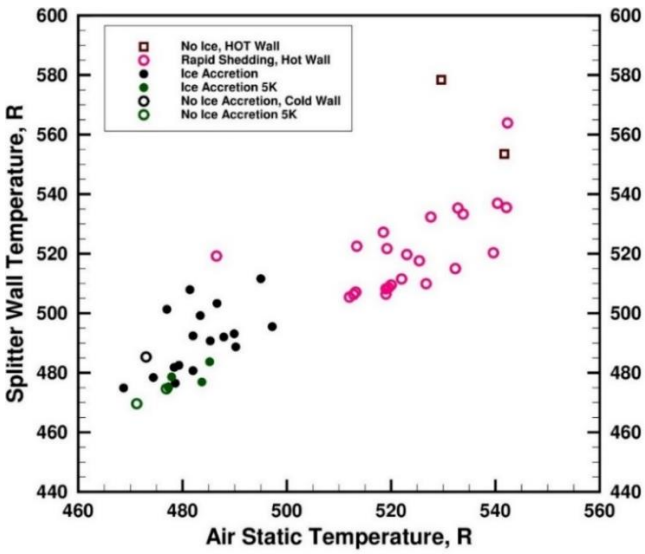

Figure 16. Calculated wall temperature at the splitter-shroud wall region versus calculated air static temperature.

VARIABLE INLET GUIDE VANE (IGV) REGION

As in the splitter-lip-shroud region, the Icing Wedge thresholds are likewise not applicable in the IGV region as an indicator of accretion risk. This is likewise due to the additional heat flux through the wall at the splitter-lip-shroud region that may provide liquid water to the IGV. Accretion occurred on the IGV at test data points which had calculated Twbs from 33.4R to 19.4R below freezing, while the calculated static air temperatures were from 4R to 23R below freezing. The range of measured metal temperature of the IGV was near 492R. Table 4 shows the analysis results for Escort 284, with the measured IGV metal temperature of 502R before ice cloud initiation, and 491R 60 seconds after ice cloud was initiated.

Table 4 Typical IGV Data Point with Ice Accretion

Escort Data Point	Altitude, K ft	Flight Mach	Ambient Temp, R	Tt PSL Station 1 Ice Cloud ON, R	Pt PSL Station1, psia	Ice Water Content (IWC)	IWAR	Twbs, IGV Station 8	T- Metal IGV 2.5 Pre Ice, R	T - Metal IGV 2.5 Post Ice; 60s, R
284	36	0.61	412.8	443.4	4.21	4.10	0.0105	469.6	502.1	490.6

Figure 17 shows the video image of ice accretion on the IGV for Escort data point 284. The ice accreted near the tip region.

Figure 17. Ice accretion on the IGV surface near the tip (Escort 284 at 36K ft altitude).

Accretion on the IGV appeared to be a function of IWAR for all test points. For all test points the minimum limit where ice accretion occurred had IWAR values above 0.008 (Figure 18).

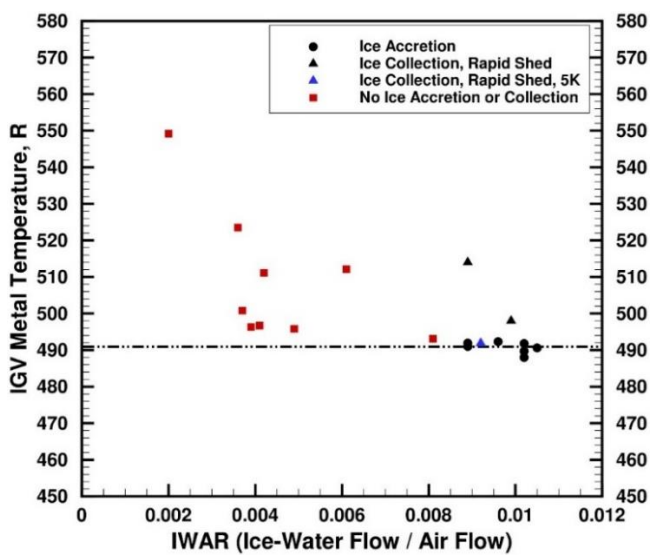

Figure 18. Measured IGV metal temperatures versus IWAR for all operating points with video confirmation.

UNCERTAINTY

Key HURE engine performance parameters from the CD system model were compared to the Escort measurement data in order to validate the model. Figure 19 illustrates the percentage difference of the parameters between the measured Escort data and the CD model as a function of Escort data number, which increased chronologically. Variances of up to 6% were noted for certain engine performance parameters. The analysis conducted

in this study was based on the CD estimate of the flow through the core. These differences may affect the analysis results with COMDES-MELT, thus adding to the uncertainty.

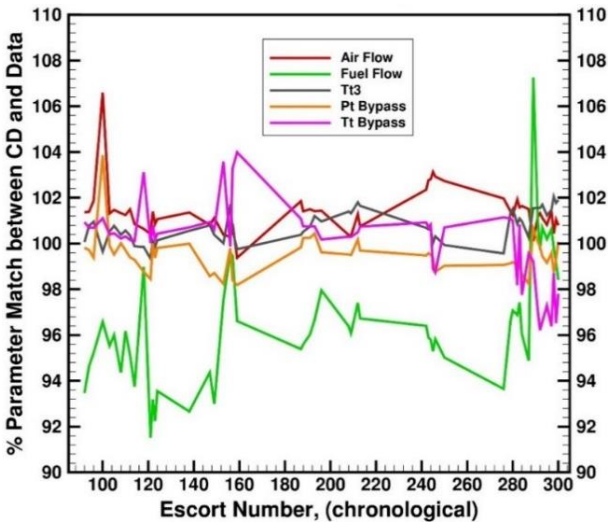

Figure 19. Percentage difference between the CD model and the Escort test data as a function of Escort number.

CONCLUSIONS

The Honeywell Uncertified Research Engine (HURE) has been tested in the Propulsion System Laboratory (PSL) at NASA Glenn Research Center with ice crystal cloud ingestion over a range of simulated altitudes, ambient temperatures, and engine operating conditions (varying flight Mach number and fan speed).

A computational process utilizing the mean-line (COMDES-MELT) aerodynamic compressor flow analysis code along with the Honeywell provided customer deck were utilized for the post-test analysis of the engine test data.

The HURE engine testing indicates that ice accretion occurred differently in the fan-stator, than it does near the splitter-lip and shroud region, as well as on the compressor inlet guide vane.

- Ice accretion on the non-metallic fan-stator vanes occurs within the range of wet bulb temperature thresholds of the Icing Wedge (492R – 498R) where it was expected to occur, and did not have any icing when the Twbs was outside these Icing Wedge thresholds. The accretion here appears to be an adiabatic process. In the fan-stator region the static wet bulb temperature thresholds of the Icing Wedge, proved to have a 94% accuracy as an indicator of icing risk. Although the mean-line flow analytical capability lacks the radial distribution of ice particles, and key icing parameters, it can be an effective tool for estimating their bulk values.

- Early during the testing phase of the HURE, real-time analysis of the data indicated that the splitter-lip and shroud region of the gooseneck may have been heated, however the heat source was not well understood. The PSL test plan was adjusted accordingly for subsequent test data points. In order to induce ice accretion near the splitter-shroud region, the target value of static wet bulb temperature was reduced by 24R to a value near 468R. This proved to be a successful technique for forcing ice to accrete in that region, in spite of the suspected non-adiabatic walls. During post-test analysis, a simple heat transfer model was developed in order to calculate the wall temperature in the splitter-shroud region at all operating conditions. The heat transfer model was incorporated into the compressor flow analysis code, for an order-of-magnitude calculation of wall temperature. In this non-adiabatic region, the Icing Wedge wet bulb temperature thresholds were not applicable as an indicator of icing risk due to the additional heat flux through the walls.

- The ice accretion on the variable inlet guide vanes (IGV) of the compressor appeared to be a strong function of the IWAR (ice-water flow rate to air flow rate ratio). Ice accretion on the IGV occurred at values of IWAR above 0.008, whereas no ice accretion on the IGV occurred below that value. In the IGV region, the Icing Wedge thresholds were not applicable as an indicator of icing risk due to the source of liquid water from upstream (splitter-lip-shroud).

- Non-adiabatic compressor flow path walls require a fully coupled multidisciplinary analysis of the conjugate heat transfer through the walls, the air flow, as well as the thermodynamic state of the ice particle, in order to determine the static wet bulb temperature distribution in the flow field.

ACKNOWLEDGMENTS

This work is supported by the Advanced Air Transport Technology Project in the NASA Advanced Air Vehicles Program, and is in response to the Engine Icing Technical Challenge. We would like to acknowledge Ashlie Flegel for leading the experimental research test and providing data for the analysis, Dr. Judith Van Zante for providing icing cloud expertise, Dr. William B. Wright (Vantage Partners, LLC.) for guidance in providing the MELT code subroutine, and Dr. Jen-Ching Tsao (Ohio Aerospace Institute) for his insights. The authors would also like to thank the entire NASA PSL staff for their dedication and support of this test. The authors also wish to thank the Honeywell team for their contributions during the engine test.

REFERENCES

[1] Mason, J. G., Chow, P., Fuleki, D. M., "Understanding Ice Crystal Accretion and Shedding Phenomenon in Jet Engines Using a Rig Test," GT2010-22550.

[2] Mason, J. G., Grzych, M., "The Challenges Identifying Weather Associated With Jet Engine Ice Crystal Icing," SAE 2011-38-0094.

[3] Goodwin, R. V., Dischinger, D. G., "Turbofan Ice Crystal Rollback Investigation and Preparations Leading to Inaugural Ice Crystal Engine Test at NASA PSL-3 Test Facility," AIAA 2014-2895.

[4] Oliver, M. J., "Validation Ice Crystal Icing Engine Test in the Propulsion Systems Laboratory at NASA Glenn Research Center," AIAA-2014-2898.

[5] Flegel, A. B., Oliver, M. J., "Preliminary Results from a Heavily Instrumented Engine Ice Crystal Icing Test in a Ground Based Altitude Test Facility," AIAA-2016-3894.

[6] Struk, P., Lynch, C. J., "Ice Growth Measurements from Image Data to Support Ice-Crystal and Mixed-Phase Accretion Testing," AIAA 2012-3036.

[7] Bartkus, T. P., Tsao, J. C., Struk, P. M., Van Zante, J. F., "Numerical Analysis of Mixed-Phase Icing Cloud Simulations in the NASA Propulsion Systems Laboratory," 8th AIAA Atmospheric and Space Environments Conference, 13-17 June, 2016, Washington D.C., AIAA.

[8] Veres, J. P., Jorgenson, P. C. E., "Prediction and Analysis of Ice Accretion in a Research Turbofan Engine With Ice Crystal Cloud Ingestion at Simulated Altitudes," NASA/TM-2017-219724 (availability restricted to U.S. government and NASA contractors).

[9] Veres, J. P., "Axial and Centrifugal Compressor Mean Line Flow Analysis Method," AIAA-2009-1641, NASA/TM—2009-215585.

[10] Veres, J. P., Jorgenson, P. C. E., Wright, W. B., Struk, P., "A Model to Assess the Risk of Ice Accretion due to Ice Crystal Ingestion in a Turbofan Engine and its Effects on Performance," AIAA 2012-3038.

[11] Veres, J. P., Jorgenson, P. C. E., "Modeling Commercial Turbofan Engine Icing Risk with Ice Crystal Ingestion," AIAA 2013-2679.

[12] Veres, J. P., Jorgenson, P. C. E., Coennen R., "Modeling Commercial Turbofan Engine Icing Risk with Ice Crystal Ingestion; Follow-On," AIAA 2014-2899.

[13] Jorgenson, P. C. E., Veres, J. P., Jones, S. M., "Modeling the Deterioration of Engine and Low Pressure Compressor Performance During a Roll Back Event due to Ice Accretion," AIAA-2014-3842.

[14] Veres, J. P., Jones, S. M., Jorgenson, P. C. E., "Performance Modeling of Honeywell Turbofan Engine Tested with Ice Crystal Ingestion in the NASA Propulsion System Laboratory," SAE-2015-01-2133.

[15] Veres, J. P., Jorgenson, P. C. E., Jones, S. M, "Modeling of Highly Instrumented Honeywell Turbofan Engine Tested with Ice Crystal Ingestion in the NASA Propulsion System Laboratory," AIAA-2016-3895.

[16] Veres, J. P., Jorgenson, P. C. E., Jones, S. M., Nili, S., "Modeling of A Turbofan Engine with Ice Crystal Ingestion in the NASA Propulsion System Laboratory," GT2017-63202.

[17] Veres, J. P., Jorgenson, P. C. E., Bommireddy, S. R., Nili, S., "Analysis of the Honeywell Uncertified Research Engine (HURE) with Ice Crystal Cloud Ingestion at Simulated Altitudes (Government Version)," NASA/TM-2018-220022 (availability restricted to U.S. government and NASA contractors).

[18] Jorgenson, P. C. E., Veres, J. P., Bommireddy, S. R., Nili, S., "Analysis of the Honeywell Uncertified Research Engine (HURE) with Ice Crystal Cloud Ingestion at Simulated Altitudes (Public Version)," NASA/TM-2018-220023.